Synthesis and Cathodoluminescence of Morphology-Tunable SiO_2 Nanotubes and ZnS/SiO_2 Core−Shell Structures Using CdSe Nanocrystals as the Seeds

Tianyou Zhai,[†,‡] Zhanjun Gu,[†,‡] Yang Dong,[†,‡] Haizheng Zhong,[†,‡] Ying Ma,[*,†] Hongbing Fu,[†] Yongfang Li,[†] and Jiannian Yao[*,†]

Beijing National Laboratory for Molecular Sciences (BNLMS), Institute of Chemistry, Chinese Academy of Sciences, Beijing 100080, People's Republic of China, and Graduate School, Chinese Academy of Sciences, Beijing 100039, People's Republic of China

Received: April 19, 2007; In Final Form: May 28, 2007

High-density, ultralong SiO_2 nanotubes were successfully synthesized by a one-step thermal evaporation process using CdSe nanocrystals as the seeds. The as-synthesized products were characterized using X-ray diffraction, scanning electron microscopy, transmission electron microscopy, energy-dispersive X-ray spectrometry, and cathodoluminescence. Varying experimental parameters results in the formation of additional SiO_2-based nanostructures, such as flowerlike SiO_2 nanotubes and ZnS/SiO_2 core−shell structures. On the basis of these observations, a template-based growth mechanism was proposed for the growth of these nanostructures. Furthermore, the stable and strong visible-light emission properties are of significant interest for their potential applications in future integrated devices.

Introduction

Hollow inorganic nanotubes are attracting a great deal of attention due to their unique properties, such as the structural versatility, and the anisotropic chemical and physical properties, which make them promising materials for advanced technologies.[1,2] They also have potential applications in fields such as electronics, optics, advanced catalysis, and energy storage/conversion and could be designed to mimic biological channels.[3,4] Different types of inorganic nanotubes, such as C,[1,5] GaN,[6−8] ZnO,[9,10] ZnS,[11,12] and SiO_2, the so-called functional materials, have so far been prepared by various approaches including hydrothermal method, sol−gel technique,[13] templated-assistance method,[14−17] electroless deposition,[18] surfactant intercalation method, and thermal evaporation method.[19] Among them, template-based methods offer various advantages,[20,21] especially to produce tubular structures with monodisperse diameters and lengths as well as tunable inner and outer walls. Yang and co-workers[7] have prepared GaN nanotubes by "epitaxial casting" in which hexagonal ZnO nanowires were used as templates for epitaxial overgrowth of thin GaN sheaths, and the ZnO nanowire templates were subsequently removed by thermal reduction and evaporation with formation of GaN tubular nanostructures. Other nanotubes, such as Si,[22] ZnS,[23] and Cd_3P_2,[24] have been obtained by using the same concept.

Silica nanotubes are of special interest because of their hydrophilic nature, easy colloidal suspension formation, and surface functionalization accessibility for both inner and outer walls.[16,25,26] Furthermore, silica nanotubes have the characteristic of their room-temperature light-emission properties in the visible range and can be used for hosting materials in bioanalysis and bioseparation and potential materials in optoelectronic nanodevices.[27−36] With these unique properties and potential applications, it is desirable to develop a method for synthesizing uniformly sized and morphology-controlled silica nanotubes in bulk quantities.[37] Up to now, researchers have been extensively studying efficient synthetic routes to prepare silica nanotubes with controlled size and shape. These methods include gas-phase syntheses utilizing vapor−liquid−solid method, chemical vapor deposition, thermal evaporation, and liquid-phase syntheses involving sol−gel method[29] or organic gelators' technique.[38] The gas-phase synthetic approach is an especially powerful tool for the convenient and reproducible shaped-controlled synthesis of nanomaterials. For example, Shen et al. produced SiO_2 nanotubes based on the high-temperature (1450 °C) reaction between ZnS, SiO, and GaN.[28,39] Zhang et al. prepared silica nanotubes by reacting ZnS with Si wafers at 1300 °C.[2,40] Very recently, Lee et al. formed SiO_2 nanotubes by reducing the temperature at 1100 °C by thermal evaporation of a mixture of ZnSe or ZnS and SiO.[37,41] It is noteworthy that SiO_2-shell heterostructures were also obtained by them. However, the reaction temperature was relative high, and complicated nanostructures were rarely acquired.

For gas growth to occur, the substrate often contain a bound metal catalyst, which is typically a noble metal (i.e., gold or silver) or other type of transition metal (i.e., nickel or iron);[42] however, the behavior to use inorganic semiconductor nanocrystals as the catalyst was very limited. In recent years, we have done some research on the growth of various semiconductor nanostructures by introducing CdSe nanocrystals (NCs) into the gas-phase growth process.[43,44] Our method relies on a buffer layer of cubic CdSe NCs on the silicon substrate on which branched ZnSe nanowires and rocketlike CdS tetrapods are grown. As we know, with the additional of complex structures to nanostructures the potential for synthesizing materials with interesting electrical, optical, and mechanical properties is even greater.[45] Meanwhile, the new growth process using inorganic semiconductor nanocrystals has proved to be effective in the design and fabrication of the complex shaped and well-defined

* To whom correspondence should be addressed. Phone/Fax: +86-10-82616517. E-mail: (Y.M.) yingma@iccas.ac.cn; (J.Y.) jnyao@iccas.ac.cn.
† Institute of Chemistry, Chinese Academy of Sciences.
‡ Graduate School, Chinese Academy of Sciences.

10.1021/jp073051s CCC: $37.00
Published on Web 07/18/2007

three-dimensional architectures. Thus, this motivated us to introduce this seed-epitaxial method into other systems.

In this work, we reported the synthesis of high-density, ultralong SiO_2 nanotubes via a modified one-step chemical vapor deposition process by thermal evaporation of ZnS powder using CdSe NCs as the seeds. The main advantage of this seed-epitaxial approach is that the narrow size distribution of the products can be acquired and the morphology can be easily tuned through changing the experimental parameters. By increasing the amount of CdSe NCs, branched and flower-like SiO_2 were prepared; by decreasing the evaporation temperature, ZnS/SiO_2 core−shell structures were obtained. Interestingly, red and blue light emissions were first observed in the silica nanotubes simultaneously. It is clearly indicated that the ideal nanotubes may induce new optical properties. This result may inspire great interest in exploring other SiO_2-heterostructures and their potential applications in future integrated devices.

Experimental Section

Materials. Analytical-grade reagents including cadmium acetate, methanol, chloroform, toluene, and high-purity selenium powder (99.9%) were purchased from Beijing Chemical Reagent Ltd. Co. of China. Trioctylphosphine (TOP, 90%, Alfa), stearic acid (SA, 96%, Aldrich), and zinc sulfur powder (99.99%, Alfa) were used as received without further purification.

Synthesis of CdSe Nanocrystals (NCs). The CdSe NCs were synthesized according to the method in the literature.[46−50] Typically, the synthetic processes were carried out in an inert atmosphere and were performed using standard air-free techniques. A mixture of a specified amount of 0.46 g of $Cd(Ac)_2$ and 5.5 g of ligand SA in a 25 mL three-neck flask was heated to about 150 °C to obtain a colorless clear solution of Cd-precursor, the solution was then cooled to room temperature and aged for 24 h, and then this system was heated to 290 °C. At this temperature, 0.12 g of selenium in 2.0 mL of TOP solution was quickly injected, and then the system was reacted for 5 min at 270 °C. After the reaction, the obtained colloid solutions were cooled and precipitated by methanol. The formed flocculent precipitate was centrifuged, and the upper layer liquid was decanted; the isolated solid then was dispersed in toluene. The above centrifugation and isolation procedure was repeated several times for purification of the nanocrystals. Finally, the purified nanocrystals were redispersed in toluene. The obtained cubic nanocrystals with particle size of about 4∼5 nm were used as the seeds for the growth of SiO_2 nanotubes.

Synthesis of SiO_2 Nanotubes. The SiO_2 nanotubes were synthesized in a conventional tube furnace with a 50 mm inner-diameter quartz tube mounted inside, as described in detail elsewhere.[43,44,51] Briefly, high-purity ZnS powder was placed upstream in a quartz boat in the middle of the high-temperature zone. Single-crystal p-type Si wafers, cleaned by standard procedure and covered with a thin film of CdSe nanocrystals, were placed downstream to collect the products. After evacuation of the tube to 2×10^{-2} Torr, a carrier gas of high-purity N_2 (99.999%) was kept flowing through the tube. The flow rate and pressure inside of the tube were kept, respectively, at 60 sccm and 120 Pa throughout the experiment. The furnace was maintained at 1000 °C for 2 h before it was cooled down to room temperature. A series of samples were fabricated by varying some experimental parameters. Three representative samples (1, 2, and 3) were prepared by changing the amounts of the CdSe seeds or reaction temperatures: samples 1 and 3 were prepared at 1000 and 900 °C, respectively; sample 2 was also fabricated at 1000 °C but used more CdSe nanocrystals than for the growth of samples 1 and 3. All other experimental conditions were identical.

Measurement. The general morphology and crystallinity of these samples were characterized by scanning electron microscopy (SEM, Hitachi F-4300), X-ray diffraction (XRD, Rigaku D/max-2400PC) with Cu Kα radiation, transmission electron microscope (TEM, JEOL JEM-2010) equipped with energy-dispersive X-ray spectroscope (EDS), and high-resolution TEM (HRTEM, Philips Tecnai F30) with a Gatan image-filtering system attached. X-ray photoelectron spectrum was measured using an ESCALab220i-XL electron spectrometer from VG Scientific using 300 W Al Ka radiations. The binding energies were referenced to the C1s line at 284.6 eV from adventitious carbon. Luminescent spectra of these nanostructures were measured at room temperature by a cathodoluminescence (CL) system installed on the SEM (SEM, Quanta 200F).

Results and Discussion

SiO_2 Nanotubes (NTs). Field-emission SEM was used to examine the morphology of the products. Panels a and b of Figure 1 are the SEM images of the products obtained at 1000 °C, showing good uniformity and wirelike morphology. These nanowires have diameters of about 80∼110 nm and a length of several hundreds of micrometers. The crystal structure of the nanowires was investigated using XRD, as shown in Figure 1c. The XRD pattern shows a broad peak at $2\theta = 15\sim35°$, indicating only amorphous materials within the products. No other characteristic peaks from crystalline forms were detected in the XRD pattern. The SEM and XRD results demonstrate that the growth product is amorphous material with wirelike morphology.

Detailed microstructures and composition of the as-grown nanowires were further investigated using TEM and EDS. Figure 2 shows the TEM images of the SiO_2 nanostructures with the contrast of these images indicating the hollow structures. Typical nanotubes have smooth surfaces and uniform thickness, round cross sections for both their interiors and exteriors, and outer diameters of about 80 nm in accordance with the SEM results. Most of them have two opened ends as shown in Figure 2b. Besides the straight SiO_2 nanotubes, some interesting tubular SiO_2 nanostructures, such as zigzag-type nanotubes (Figure 2d), were also obtained under the present experimental conditions. Figure 2e shows the HRTEM image of a single SiO_2 nanotube. No lattice fringe could be observed for the nanotube, indicating its amorphous state. The corresponding selected-area electron diffraction (SAED) pattern (upper right inset of Figure 2e) shows only diffuse rings without diffraction spots, also suggesting that the as-synthesized tubes are amorphous in nature. The corresponding elemental composition is confirmed by EDS to be Si and O with an approximate atomic ratio of 1:2 (the Cu signal comes from the TEM grids), confirming these nanotubes are amorphous SiO_2.

Further evidence for the formation of SiO_2 can be obtained through X-ray photoelectron spectroscopy (XPS). Figure 3 shows spectra of these nanotubes. The survey spectrum in Figure 3a displays mainly the oxygen and silicon peaks. Quantification of these peaks reveals that the atomic ratio of O to Si is about 62.5:31.3. The presence of C comes mainly from atmospheric contamination due to the exposure of the sample to air. The binding energies in all the XPS spectra were corrected for specimen charging by reference to C1s at 284.60 eV. The two strong peaks at 103.5 and 532.7 eV, as shown in Figure 3b,c, correspond to the binding energies of Si2p and O1s for SiO_2, respectively. These results are in agreement with those reported

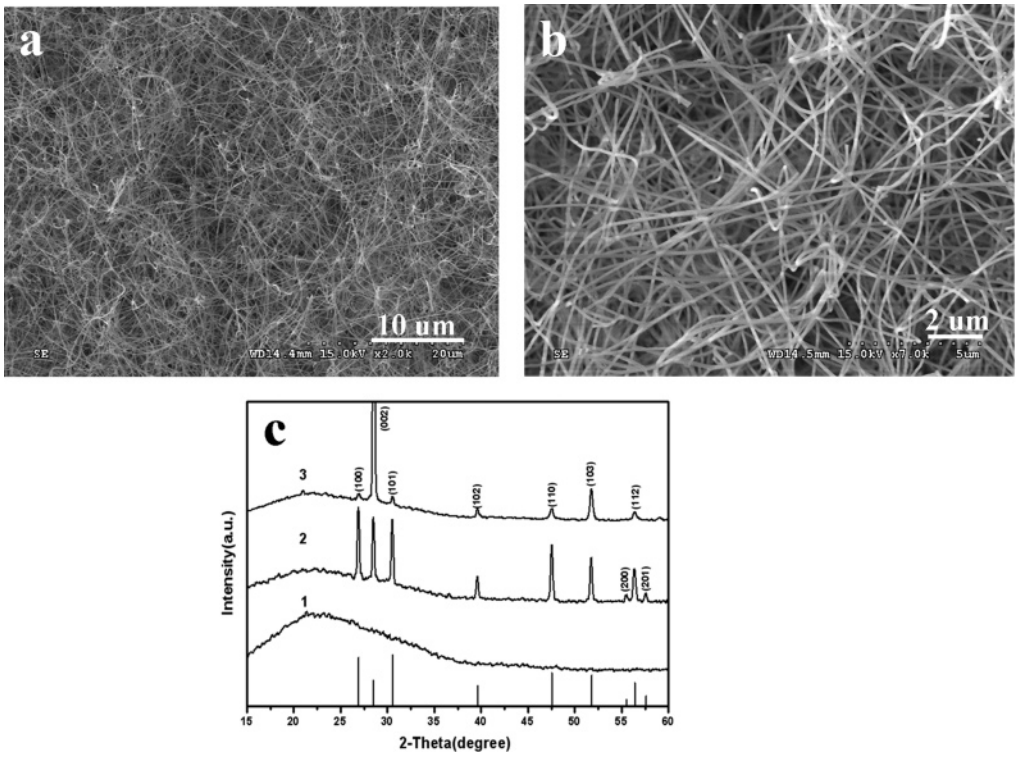

Figure 1. (a,b) SEM images of the obtained SiO_2 nanotubes (sample 1) synthesized at 1000 °C; (c) XRD patterns of the samples 1−3, respectively. The vertical lines at the bottom in Figure 1c corresponding to the standard XRD pattern of wurtzite ZnS (JCPDS No. 36−1450).

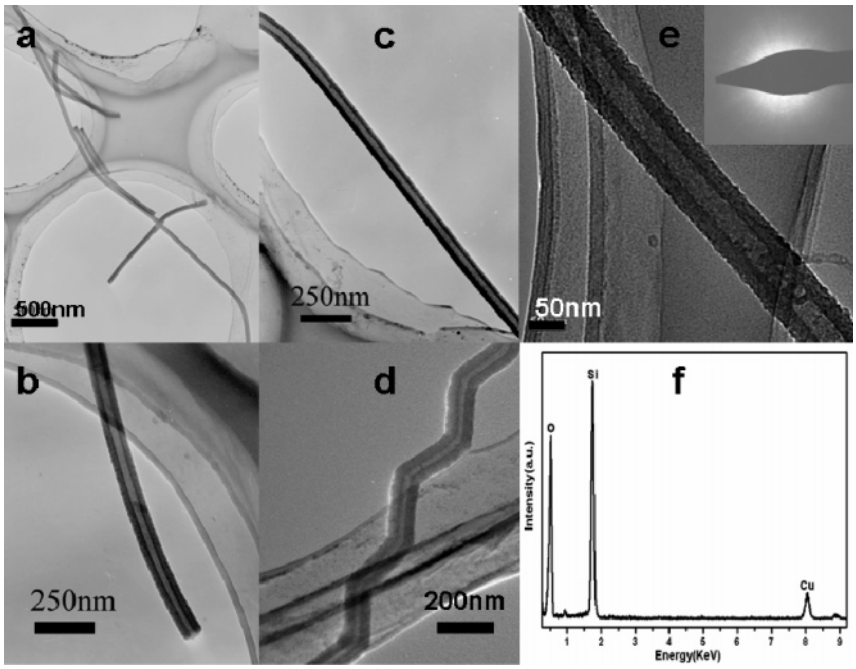

Figure 2. (a) TEM image of the obtained SiO_2 tubular nanostructures; (b) TEM image displaying the open end of a SiO_2 nanotube; (c,d) TEM images of the straight and zigzag-type SiO_2 nanotubes; (e) HRTEM image; and (f) EDS spectrum of a SiO_2 nanotube.

previously.[52−53] No obvious Si peaks (Si2p at 98.7 eV in Si) are observed. All XRD, EDS, and XPS analyses indicate that the as-prepared products are amorphous SiO_2.

During the TEM observation, we found that there are still ZnS nanowires in a few SiO_2 nanotubes. The ZnS/SiO_2 nanocables have similar dimensions as those of the SiO_2 nanotubes, implying that those ZnS/SiO_2 nanocables may represent the intermediate state of the final morphology. It should be mentioned that these nanocables are scarce as compared with the nanotubes. As seen in Figure 4a, residual segments of the ZnS nanowire remain in an open-ended SiO_2 tubular nanostructure, owning to incomplete evaporation of the ZnS nanowire (see the following discussions), which suggests that the SiO_2 tubular nanostructures are an extension of the thin SiO_2 sheath of the ZnS/SiO_2 core/shell nanowires. The different contrast between the inside and the outside of these nanowires provides significant evidence of a core−shell structure. The lower inset in Figure 4a shows the diffraction pattern and plane indices recorded from a ZnS/SiO_2 core−shell structure. The pattern indicates the single crystalline characteristic of the ZnS core nanowire and shows that it grows along the [01-10] direction. Diffusive white contrast was also observed, confirming

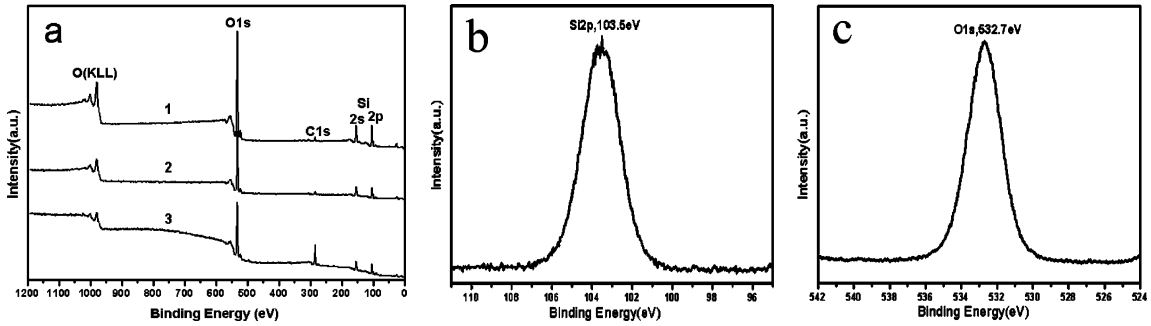

Figure 3. (a) XPS spectra of the samples 1−3, respectively; (b) Si2p binding energy spectrum; (c) O1s binding energy spectrum.

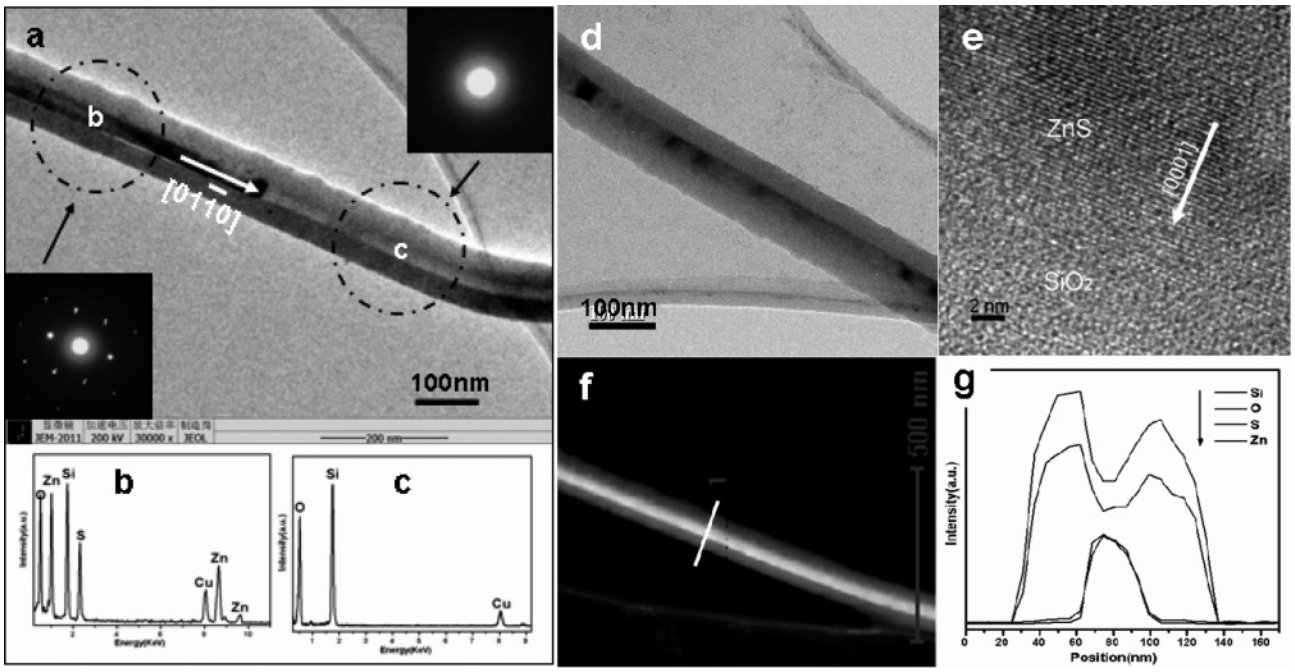

Figure 4. (a,d) TEM images showing the residual segments of the ZnS nanowire in the open-ended SiO_2 nanotubes (the insets are SAED taken from the domains indicated by arrows); (b,c) EDS spectra of the parts circled in (a); (e) HRTEM image taken from the interfacial domain between the SiO_2 shell and ZnS core of a ZnS/SiO_2 core/shell nanowire; (f) a scanning TEM image of a single nanocable; (g) line-scanning (indicated by a line in (f)) element mapping displaying Si, O, Zn, and S spatial element distribution profiles across the ZnS/SiO_2 core/shell nanowire.

that the ZnS nanowire was surrounded by a SiO_2 shell. Figure 4e shows an HRTEM image of the interfacial domain between SiO_2 shell and the ZnS core of a ZnS/SiO_2 core/shell nanowire. The HRTEM image clearly shows that the shell is amorphous, while the core ZnS is single crystalline. The observed interplanar d-spacing is 0.31 nm, corresponding well with the [0001] lattice plane spacing of wurtzite ZnS. EDS spectra recorded from both the core single crystalline nanowire and the shell further verify the chemical composition. The spectra show the appearance of Zn and S X-ray signals for the core single crystalline nanowires, along with Si and O reflections for the shell nanotubes, thus confirming that the crystalline nanowire is made of ZnS and the amorphous shell is composed of SiO_2. Figure 4f is a scanning TEM image of a single nanocable. Line-scanning element profiles across a ZnS/SiO_2 core/shell nanowire (white line in Figure 4f) are shown in Figure 4 g. The profiles of Si and O both show two peaks on the right- and left-hand sides with lower intensity in the center, whereas the profiles of Zn and S both show a broad peak in the center that further verifies the core/shell nature of the ZnS/SiO_2 nanowires.

Flowerlike SiO_2 Nanotubes (SiO_2 FNTs). A similar one-step evaporation approach was used to grow flowerlike SiO_2 nanotubes (sample 2), except that an excess of CdSe nanocrystals (in comparison with that of sample 1) was used; Figure 1c shows the XRD of the as-grown products. Apart from the broad peak, all other strong peaks can be readily indexed to hexagonal wurtzite ZnS structures, that is, sample 2 is a composite material of amorphous SiO_2 and hexagonal ZnS, and their morphology differs tremendously, as shown in Figure 5. From these images, it can be seen that the products possess interesting flowerlike nanostructures. The high-magnification image shows that the diameters and the lengths of these nanotubes have little change compared with that of sample 1; however, some flowerlike structures were obtained in these nanostructures. Figure 6 gives the TEM images of these products. The flowerlike nanostructures usually have four pods with a diameter of 100 nm and a length of 200 nm. Branched nanotubes were also formed in this work that could provide interesting implications in fluidic applications, as shown in Figure 6b,e. High-magnification TEM images shown in Figure 6c,d indicate the flowerlike parts were almost hollow. The SAED pattern inset in Figure 6e also shows the amorphous state of these nanotubes. Analysis by EDS recorded from the flowerlike part confirms that they are SiO_2 with a minimal content of ZnS.

ZnS/SiO_2 Core−Shell Structures. Different nanostructures were fabricated at lower temperature (900 °C) than for the growth of sample 1, while keeping the other experimental

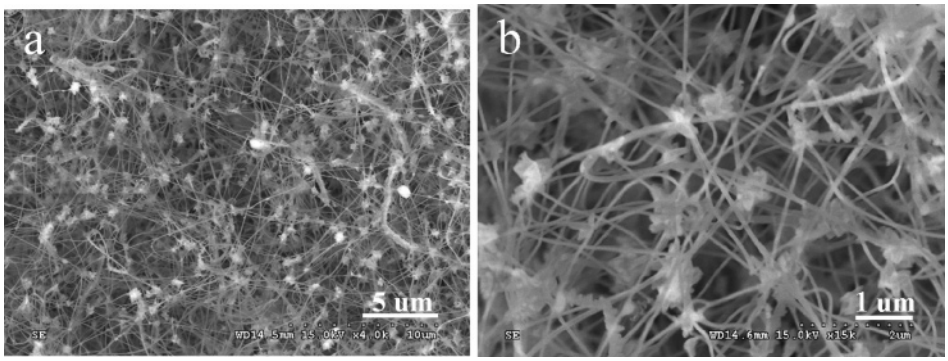

Figure 5. SEM images of the flowerlike SiO_2 nanotubes (sample 2) obtained using more CdSe nanocrystals.

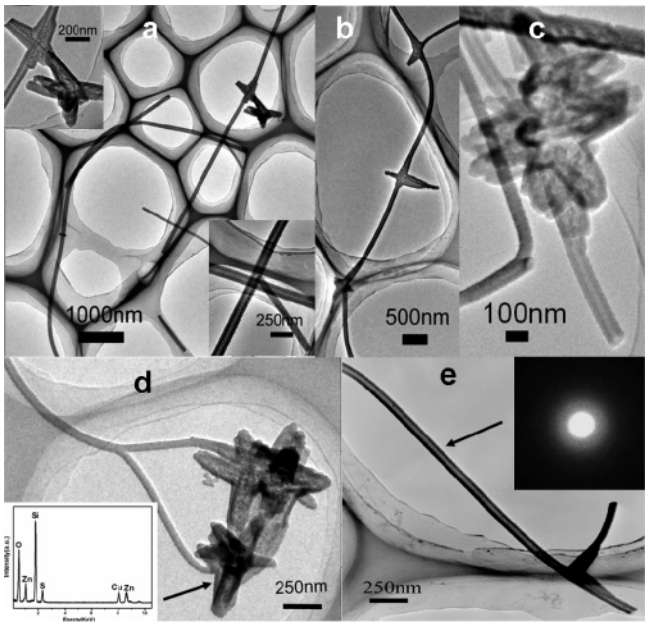

Figure 6. TEM images of the flowerlike SiO_2 nanotubes.

conditions identical. Figure 1c shows the XRD pattern of the as-grown product (sample 3), indicating the same XRD peak positions as those in sample 2. The morphology of sample 3 was different from that of sample 1 and 2, as shown in Figure 7. The SEM images indicate that the diameters and lengths of the structures changed dramatically, and the surfaces were not smooth compared with those of the nanotubes. Figure 8a,b shows the TEM images of these products. The TEM images reveal that numerous nanobranches, which linked with each other forming the shell, grew on the core nanowires, and the clear contrast variations between the outer part and the inner part indicates that these nanowires are novel core−shell structures. The inner nanowires have diameters of 80∼100 nm, and the thickness of the outer layers ranges from 100 to 150 nm. The ED pattern taken from the core part is similar to that of the residual ZnS/SiO_2 nanowires in sample 1, that is, diffusive ring and well-correlated diffraction spots correspond to amorphous SiO_2 and single-crystalline ZnS, respectively. The diffraction patterns recorded from the different parts along the wire length are exactly the same, showing the single crystalline nature of the entire filled ZnS nanowire. The HRTEM image also confirms the ZnS core is a single crystalline structure growing along [01-10] direction. EDS spectra taken from the core and the shell parts confirm that the shell is SiO_2 and the core is ZnS. The corresponding XPS spectrum was also investigated (Figure 3a). Only peaks of Si and O are present in the spectrum,-without any peaks for Zn and S. The complete disappearance of the Zn and S peaks further proves that the ZnS nanowires are completely surrounded by a SiO_2 layer.

Growth Mechanism. On the basis of all the above analysis, the template-based growth of the silica nanotubes is proposed. The above findings suggest that the two-stage processes are responsible for the formation of the silica nanotubes. It is believed that the nanocables of SiO_2-sheathed ZnS were first achieved in the experiments. It is worth mentioning that no SiO_2 nanostructure growth was observed on the same substrate in the absence of either ZnS powder or CdSe nanocrystals. At the beginning, the CdSe NCs serve as the nuclei and reduce the interface energy barrier for the crystal growth of the ZnS nanowires. In general, surface nucleation is favored when the crystal/surface interfacial free energy is low. As we know, deposition of a seed layer helps to promote surface nucleation.[54] Furthermore, CdSe and ZnS have similar structures,[55] and an effective epitaxial growth would be preferred to minimize the interface lattice mismatch. These behaviors are well known, and similar phenomena were observed by Wang et al.[56] Because of the anisotropic nature of wurtzite ZnS phases, 1D ZnS nanowires are rapidly formed. Because of the relative good epitaxial lattice match between the wurtzite ZnS (010) plane and cubic CdSe (111) plane, the ZnS nanowires probably grow along the [01-10] direction, which is different from the conventional [0001] orientation. Subsequently, some CdSe nanocrystals may be transported from another place and adsorbed on the side of the nanowires. These CdSe nanocrystals are energetically favored sites for the adsorption of incoming ZnS vapors. Epitaxial growth again occurs on the seeds, so branched or flowerlike nanowires may be formed. Meanwhile, the surface of the silicon was oxidized to form SiO_x (the trace remnant of oxygen that was not eliminated completely by flushing with N_2 and/or from the leakage of the furnace serves as the oxidant) during heating. In this stage, the ZnS nanowire serves as the preferable adsorption site for the SiO_x in the vapor phase and eventually works as the template for the growth of SiO_2. The SiO_x vapor surrounding ZnS nanowires was oxidized to form SiO_2 and was deposited on the outer surfaces of the ZnS nanowires, resulting in the formation of ZnS-core/SiO_2-shell nanocable heterostructures (Figure 9c). This is supported by two experimental facts: (1) No extra silicon and oxygen sources are provided. (2) The nanotubes are only found on the silicon substrate, indicating the Si substrate is the Si source. Because of the high temperature, the ZnS nanowires inside are partially consumed through evaporation out of the coaxial nanocables, whereas the SiO_2 shell remains intact and amorphous SiO_2 nanotubes with circular cross sections are formed (Figure 9d). The proposed mechanism is supported by the fact that the residual segment of the ZnS nanowires template remains in the open-ended silica nanotubes, and the residual ZnS content in the flowerlike SiO_2 nanotubes

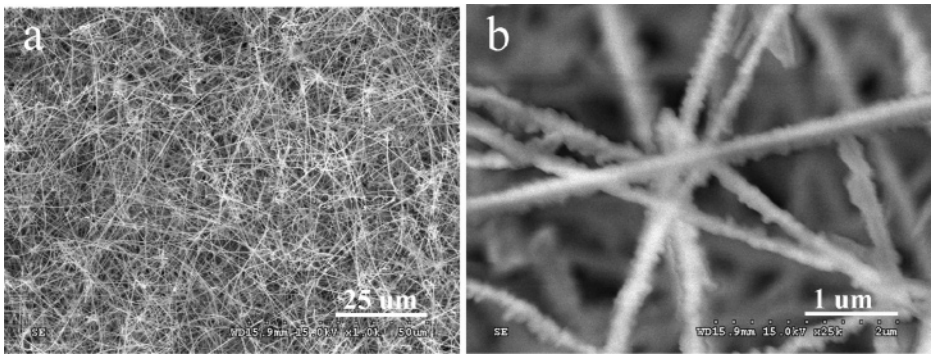

Figure 7. SEM images of ZnS/SiO_2 core−shell structures (sample 3) obtained at 900 °C.

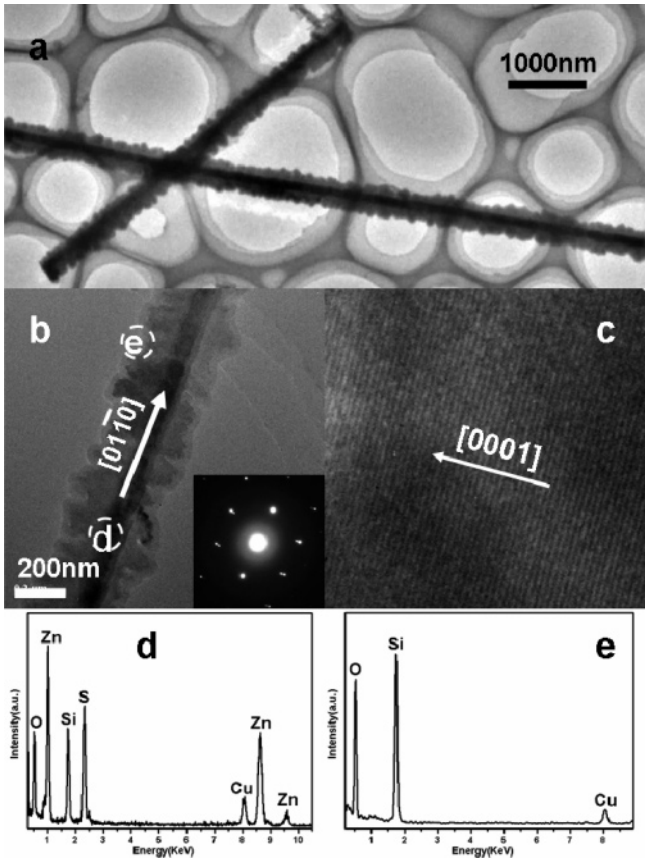

Figure 8. (a,b) TEM images of the ZnS/SiO_2 core−shell structures; (c) HRTEM image taken from the core part; (d,e) EDS spectra taken from the core and the shell parts marked in Figure 8b, respectively.

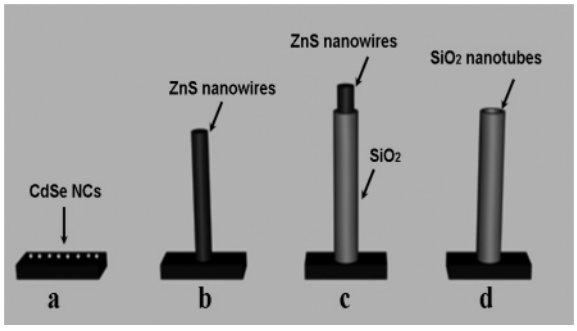

Figure 9. Proposed growth mechanism of the SiO_2 nanotubes, see text for details.

were more than that in the SiO_2 nanotubes because the branched or flowerlike structures are unfavorable for the diffusion of ZnS. A similar mechanism has been used to explain the growth of Si nanotubes[22] and Zn_3P_2 nanotubes.[24]

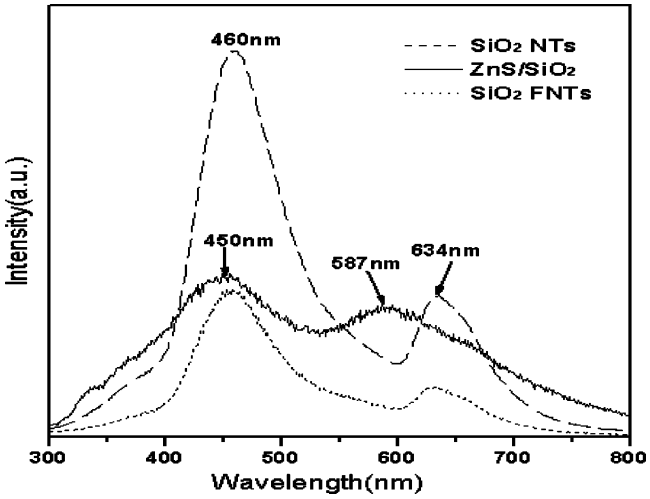

Figure 10. Room-temperature cathodoluminescence spectra of the SiO_2 nanotubes (dashed line), flowerlike SiO_2 nanotubes (dotted line), and ZnS/SiO_2 core−shell structures (solid line) obtained with a focused electron beam at an accelerating voltage of 15 kV, respectively.

Cathodoluminescence (CL). To investigate the optical properties of the as-synthesized SiO_2 nanotubes, the nanoscale CL spectroscopy and CL imaging were conducted at an acceleration voltage of 15 KV. To visualize the spatial distribution of luminescence from these structures, CL images were recorded at room temperature, as shown in Figure S2 in Supporting Information. In the CL images, all the nanostructures appear bright. As can be seen from the dashed line, the as-grown SiO_2 nanotubes display a strong blue emission at about 460 nm (2.70 eV) and a weak red emission at about 634 nm (1.95 eV). As we know, both distinct CL bands corresponding to red and blue light emissions are first observed in the silica nanostructures simultaneously. The strong blue emission at 460 nm is similar to the result for the amorphous silica nanowires synthesized using the laser ablation approach.[57] However, it was different from the emission bands of silica nanotubes prepared by the sol−gel template method (SGTM)[29,53] Zhang et al.[53] observed the emissions centered at 486 nm, and Jang et al.[29] found the emissions centered at 435 nm with shoulders at 410 and 460 nm. Compared with the emissions previously reported, the intensive peak at 435 nm in ref 29 disappears in Figure 10 while the shoulder at 460 nm changes into the intensive peak. This phenomenon indicates that the luminescence characteristic depends strongly on the silica structure, which is affected by the synthetic variables.

The luminescence of various silica glasses and nanostructures has been studied extensively, because amorphous SiO_2 films are widely used as passivation or insulation layers in integrated circuits.[35] Several luminescence bands in various silica glasses

and nanostructures with different peak ranging from 1.6 to 4.3 eV have been obtained from both experimental measurements and theoretical calculations.[58,59] For example, the 2.7 eV band is ascribed to the neutral oxygen vacancy (≡Si−Si≡), and the 3.0 eV band corresponds to some intrinsic diamagnetic defect center, such as the two-fold-coordinated silicon lone-pair centers (O−Si−O).[60] These defects are clearly due to high oxygen deficiency. These structure defects are radiative recombination centers. Blue luminescence was also observed in Si^+-implanted SiO_2 films peaking at around 2.7 eV, which was believed to be due to oxygen vavancy.[61] It is therefore reasonable for us to believe that the very intensive blue light emission from the SiO_2 nanotubes can be attributed to the abovementioned defect centers arising from the oxygen deficiency.

Awazu and Kawazoe[62] have assigned the 1.95-eV band to the photodissociation of O_3 in oxygen-surplus silica; however, the O_3 model can be ruled out because the obtained silica nanotubes in our system do not contain surplus oxygen. Other workers assigned it to the nonbridging oxygen hole center (NBOHC, ≡Si−O•).[58,63−65] The NBOHC-induced band was observed in the oxygen-surplus silica and the high-OH silica. For our oxygen-deficient and no −OH sample, it is possible for the NBOHC (≡Si−O•) to be induced by the high-energy electron excitation in our CL measurement:

$$\equiv\text{Si-O-O-Si}\equiv \rightarrow 2(\equiv\text{Si-O}\bullet)$$

It is thought that subsequent excitation of the NBOHCs results in the 1.95 eV luminescence.

The CL spectrum of flowerlike SiO_2 nanotubes reveals also two strong emission peaks at around 456 and 630 nm, a little blue-shifted with respect to the emissions of SiO_2 nanotubes. In the case of the ZnS/SiO_2 core−shell nanostructures, the CL spectrum consists of two broad bands centered at 450 nm (2.76 eV) and 587 nm (2.11 eV), respectively. Compared with the emission bands of the SiO_2 nanotubes, the blue emission band shows a relatively low intensity and a little blue shift of about 10 nm, while the green emission band becomes stronger compared to the blue one and shows a marked blue shift of about 47 nm, which might be due to the effect of the inner ZnS nanowires. The emission at 587 nm may originate from some self-activated centers, vacancy states, element sulfur species on the ZnS surface, or interstitial states associated with the peculiar nanostructures according to the previous reports,[39] the nature of which is not clear or worthy of further study.

Conclusions

In conclusion, high-density, ultralong SiO_2 nanotubes were fabricated via a one-step seed-epitaxial thermal evaporation process using CdSe nanocrystals as the seeds. A template-based growth mechanism is proposed to explain the nanotubes formation, which involves the in situ step-by-step formation of ZnS nanowires, ZnS/SiO_2 nanocables, and finally SiO_2 nanotubes. By carefully controlling the experimental parameters, flowerlike SiO_2 nanotubes and ZnS/SiO_2 core−shell structures can be effectively obtained through changing the amounts of CdSe seeds and the evaporation temperature, respectively. This seed-epitaxial method results in fairly uniform ZnS nanowires, which leads to the narrow size distribution of the nanotubes. Although the detailed growth mechanism requires more systematic investigations, the present results suggest that this simple method might be useful for the synthesis of pure SiO_2 nanotubes with tunable-morphology and/or other SiO_2-shell heterostructures. Furthermore, the stable and strong visible-light emissions of these as-grown products are of significant interest for their potential applications in future integrated devices.

Acknowledgment. This work was supported by National Natural Science Foundation of China (No. 50221201, 90301010, 50502033), the Chinese Academy of Sciences, National Basic Research Program of China (No. 2006CB806200), and National High-tech R&D program (863 Program)(2006AA03Z314).

Supporting Information Available: XRD pattern and TEM image of the CdSe nanocrystals, and CL images of the samples 1−3. This material is available free of charge via the Internet at http://pubs.acs.org.

References and Notes

(1) Iijima, S. *Nature* **1991**, *354*, 56.
(2) Li, Y.; Ye, C. H.; Zhang, L. D.; Fang, X. S.; Zhang, Y. G. *Chem. Lett.* **2004**, *33*, 1638.
(3) Haradam, M.; Adachi, M. *Adv. Mater.* **2000**, *12*, 839.
(4) Zhou, J.; Liu, J.; Yang, R.; Lao, S. C.; Gao, P. X.; Tummala, R.; Xu, N. S.; Wang, Z. L. *Small* **2006**, *2*, 1344.
(5) Amelinckx, S.; Zhang, X. B.; Braerts, D.; Zhang, X. F.; Ivanov, V.; Nagy, J. B. *Science* **1994**, *265*, 635.
(6) Hamilton, E. J. M.; Dolan, S. E.; Mann, C. E.; Colijin, H. O.; McDonald, C. A.; Shore, S. G. *Science* **1993**, *260*, 659.
(7) Goldberger, J.; He, R. R.; Zhang, Y. F.; Lee, S.; Yan, H. Q.; Choi, H. J.; Yang, P. D. *Nature* **2003**, *422*, 599.
(8) Dinesh, J.; Eswaramoorthy, M.; Rao, C. N. R. *J. Phys. Chem. C* **2007**, *111*, 510.
(9) Sun, Y.; Fuge, G. M.; Fox, N. A.; Riley, D. J.; Ashfold, N. R. *Adv. Mater.* **2005**, *17*, 2477.
(10) Kong, X. Y.; Ding, Y.; Wang, Z. L. *J. Phys. Chem. B* **2004**, *108*, 570.
(11) Zhai, T. Y.; Gu, Z. J.; Ma, Y.; Yang, W. S.; Zhao, L. Y.; Yao, J. N. *Mater. Chem. Phys.* **2006**, *100*, 281.
(12) Yan, C.; Xue, D. *J. Phys. Chem. B* **2006**, *110*, 25850.
(13) Kovtyukhova, N. I.; Mallouk, T. E.; Mayer, T. S. *Adv. Mater.* **2003**, *15*, 780.
(14) Niu, H. J.; Gao, M. Y. *Angew. Chem., Int. Ed.* **2006**, *45*, 6462.
(15) Chueh, Y. L.; Chou, L. J.; Wang, Z. L. *Angew. Chem., Int. Ed.* **2006**, *45*, 7773.
(16) Fan, R.; Wu, Y. Y.; Li, D. Y.; Yue, M.; Majumdar, A.; Yang, P. D. *J. Am. Chem. Soc.* **2003**, *125*, 5254.
(17) Fan, H. J.; Knez, M.; Scholz, R.; Nielsch, K.; Pippel, E.; Hesse, D.; Zacharias, M.; Gösele, U. *Nat. Mater.* **2006**, *5*, 627.
(18) Yan, C. L.; Xue, D. F. *Electrochem. Commun.* **2007**, *9*, 1247.
(19) Hu, J. Q.; Meng, X. M.; Jiang, Y.; Lee, C. S.; Lee, S. T. *Adv. Mater.* **2003**, *15*, 70.
(20) Martin, C. R. *Science* **1994**, *266*, 1961.
(21) Parthasarathy, R.; Martin, C. R. *Nature* **1994**, *369*, 298.
(22) Hu, J. Q.; Bando, Y.; Liu, Z. W.; Zhan, J. H.; Golberg, D.; Sekiguchi, T. *Angew. Chem., Int. Ed.* **2004**, *43*, 63.
(23) Liu, Z. Q.; Zhang, D. H.; Han, S.; Li, C.; Lei, B.; Lu, W. G.; Fang, J. Y.; Zhou, C. W. *J. Am. Chem. Soc.* **2005**, *127*, 6.
(24) Shen, G. Z.; Bando, Y.; Ye, C. R.; Yuan, X. L.; Sekiguchi, T.; Golberg, D. *Angew. Chem., Int. Ed.* **2006**, *45*, 7568.
(25) Xiao, Z. D.; Zhang, L. D.; Meng, G. W.; Tian, X. K.; Zeng, H. B.; Fang, M. *J. Phys. Chem. B* **2006**, *110*, 15724.
(26) Van Bommel, K. J. C.; Friggeri, A.; Shinkai, S. *Angew. Chem., Int. Ed.* ***2003***, *42*, *980*.
(27) Mitchell, D. T.; Lee, S. B.; Trofin, L.; Li, N. C.; Nevanen, T. K.; Soderlund, H.; Martin, C. R. *J. Am. Chem. Soc.* **2002**, *124*, 11864.
(28) Shen, G. Z.; Bando, Y.; Golberg, D. *J. Phys. Chem. B* **2006**, *110*, 23170.
(29) Jang, J.; Yoon, H. *Adv. Mater.* **2004**, *16*, 799.
(30) Zygmunt, J.; Krumeich, F.; Nesper, R. *Adv. Mater.* **2003**, *15*, 1538.
(31) Li, F.; Wang, Z. Y.; Stein, A. *Angew. Chem., Int. Ed.* **2007**, *46*, 1885.
(32) Li, Y. B.; Bando, Y.; Golberg, D.; Uemura, Y. *Appl. Phys. Lett.* **2003**, *83*, 3999.
(33) Lee, S. B.; Mitchell, D. T.; Trofin, L.; Nevanen, T. K.; Söderlund, H.; Martin, C. R. *Science* **2002**, *296*, 2198.
(34) Wang, Z. L.; Gao, R. P.; Gole, J. L.; Stout, J. D. *Adv. Mater.* **2000**, *12*, 1938.
(35) Meng, G. W.; Peng, X. S.; Wang, Y. W.; Wang, C. Z.; Wang, X. F.; Zhang, L. D. *Appl. Phys. A* **2003**, *76*, 119.
(36) Yu, D. P.; Hang, Q. L.; Ding, Y.; Zhang, H. Z.; Bai, Z. G.; Wang, J. J.; Zou, Y. H.; Qian, W.; Xiong, G. C.; Feng, S. Q. *Appl. Phys. Lett.* **1998**, *73*, 3076.

(37) Fan, X.; Meng, X. M.; Zhang, X. H.; Lee, C. S.; Lee, S. T. *Appl. Phys. Lett.* **2007**, *90*, 103114.
(38) Jung, J. H.; Ono, Y.; Shinkai, S. *Angew. Chem., Int. Ed.* **2000**, *39*, 1862.
(39) Shen, G. Z.; Bando, Y.; Tang, C. C.; Golberg, D. *J. Phys. Chem. B* **2006**, *110*, 7199.
(40) Li, Y.; Ye, C. H.; Fang, X. S.; Yang, L.; Xiao, Y. H.; Zhang, L. D. *Nanotechnology* **2005**, *16*, 501.
(41) Fan, X.; Meng, X. M.; Zhang, X. H.; Wu, S. K.; Lee, S. T. *Appl. Phys. Lett.* **2005**, *86*, 173111.
(42) Mieszawska, A. J.; Jalilian, R.; Sumanasekera, G. U.; Zamborini, F. P. *Small* **2007**, *3*, 722.
(43) Zhai, T. Y.; Gu, Z. J.; Zhong, H, Z.; Dong, Y.; Ma, Y.; Fu, H. B.; Li, Y. F.; Yao, J. N. *Cryst. Growth Des.* **2007**, *7*, 488.
(44) Zhai, T. Y.; Zhong, H. Z.; Gu, Z. J.; Peng, A. D.; Fu, H. B.; Ma, Y.; Li, Y. F.; Yao, J. N. *J. Phys. Chem. C* **2007**, *111*, 2980.
(45) Wan, Q.; Wei, M.; Zhi, D.; MacManus-Driscoll, J. L.; Blamire, M. G. *Adv. Mater.* **2006**, *18*, 234.
(46) Li, Y. C.; Zhong, H. Z.; Li, R.; Zhou, Y.; Yang, C. H.; Li, Y. F. *Adv. Funct. Mater.* **2006**, *16*, 1705.
(47) Peng, Z. A.; Peng, X. G. *J. Am. Chem. Soc.* **2002**, *124*, 3343.
(48) Peng, X. G.; Manna, L.; Yang, W. D.; Wlckham, J.; Scher, E.; Kadavanlch, A.; Alivisatos, A. P. *Nature* **2000**, *404*, 59.
(49) Murray, C. B.; Norris, D. J.; Bawendi, M. G. *J. Am. Chem. Soc.* **1993**, *115*, 8706.
(50) Peng, Z. A.; Peng, X. G. *J. Am. Chem. Soc.* **2001**, *123*, 183.
(51) Zhai, T. Y.; Zhang, X. Z.; Yang, W. S.; Ma, Y.; Wang, J. F.; Gu, Z. J.; Yu, D. P.; Yang, H.; Yao, J. N. *Chem. Phys. Lett.* **2006**, *427*, 371.
(52) Ran, G. Z.; You, L. P.; Dai, L.; Liu, Y. L.; Lv, Y.; Chen, X. S.; Qin, G. G. *Chem. Phys. Lett.* **2004**, *384*, 94.
(53) Zhang, M.; Ciocan, E.; Bando, Y.; Wada, K.; Cheng, L. L.; Pirouz, P. *Appl. Phys. Lett.* **2002**, *80*, 491.
(54) Lin, J. C.; Yates, M. Z. *Chem. Mater.* **2006**, *18*, 4137.
(55) Talapin, D. V.; Mekis, I.; Götzinger, S.; Kornowski, A.; Benson, O.; Weller, H. *J. Phys. Chem. B* **2004**, *108*, 18826.
(56) Moore, D. F.; Ding, Y.; Wang, Z. L. *J. Am. Chem. Soc.* **2004**, *126*, 14372.
(57) Wu, X. C.; Song, W. H.; Wang, K. Y.; Hu, T.; Zhao, B.; Sun, Y. P.; Du, J. J. *Chem. Phys. Lett.* **2001**, *336*, 53.
(58) Nishikawa, H.; Shiroyama, T.; Nakamura, R.; Ohki, Y.; Nagasawa, K.; Hama, Y. *Phys. Rev. B* **1992**, *45*, 586.
(59) Yang, Y.; Tay, B. K.; Sun, X. W.; Fan, H. M.; Shen, Z. X. *Physica E* **2006**, *31*, 218.
(60) Tohmon, R.; Mizuno, H.; Ohki, Y.; Sasagane, K.; Nagasawa, K.; Hama, Y. *Phys. Rev. B* **1989**, *39*, 1337.
(61) Liao, L. S.; Bao, X. M.; Li, N. S.; Min, N. B. *Appl. Phys. Lett.* **1996**, *68*, 850.
(62) Awazu, K.; Kawazoe, H. *J. Appl. Phys. B* **1990**, *68*, 3584.
(63) Skuja, L. N.; Silin, A. R. *Phys. Status Solidi A* **1979**, *56*, K11.
(64) Munekuni, S.; Yamanaka, T.; Shimogaichi, Y.; Tohmon, R.; Ohki, Y.; Nagasawa, K.; Hama, Y. *J. Appl. Phys.* **1990**, *68*, 1212.
(65) Glinka, Y. D.; Lin, S. H.; Chen, Y. T. *Phys. Rev. B* **2000**, *62*, 4733.